Energy & Environmental Science

ROYAL SOCIETY OF CHEMISTRY

PAPER

Cite this: *Energy Environ. Sci.*, 2021, **14**, 1563

Revealing defective nanostructured surfaces and their impact on the intrinsic stability of hybrid perovskites†

Yuze Lin, ‡[a] Ye Liu,‡[ab] Shangshang Chen, [a] Shen Wang,[a] Zhenyi Ni,[a] Charles H. Van Brackle,[a] Shuang Yang,[a] Jingjing Zhao,[a] Zhenhua Yu,[a] Xuezeng Dai,[a] Qi Wang,[a] Yehao Deng[a] and Jinsong Huang *[ab]

Received 12th January 2021,
Accepted 25th January 2021

DOI: 10.1039/d1ee00116g

rsc.li/ees

The instability of metal halide perovskites (MHPs) remains to be one major obstacle for the commercialization of perovskite solar cells. Here we report the observation of nanocrystals and some amorphous phases at the surface of apparent single crystalline grains in polycrystalline films deposited by almost all known solution deposition methods, which accelerate the degradation of MHPs. By removing the defective surface layer through mechanical polishing, the stability of perovskite films is significantly enhanced. Encapsulated solar cells based on polished MHPs retain 93% of their initial efficiency after continuous illumination for 2180 hours at 1 sun intensity and with ultraviolet radiation at 65 °C. Removing the defective surface layers restores the mechanical hardness to be comparable to that of single crystals, which suppresses ion migration and permeation of detrimental species into perovskite grains. This study narrows down the stability gap between the MHP polycrystalline films and single crystal perovskites which represents the upper limit for the stability of MHPs.

Broader context

Revealing the origin of intrinsic instability for metal halide perovskites (MHPs) and then prolonging their lifetimes are crucial for their application in MHP electronic devices, such as solar cells, photo/radiation detectors, and light-emitting diodes, with rapidly improved efficiencies or sensitivities. As a typical example, MHP solar cells have shown high efficiencies over 25%, which continue to compete with other photovoltaic technologies, like single crystal silicon solar cells, with a promise to further decrease the cost of clean solar energy. However, the stability of MHP solar cells is still far worse than that of commercial silicon solar cells, and thus much more improvement of the stability of perovskite solar cells is in urgently needed. In this study, we observe defective nanostructured surfaces on polycrystalline MHP thin films, which accelerate the degradation of MHPs. Removing these defective surface layers by mechanical polishing restores the single-crystal like mechanical hardness, which suppresses ion migration and stabilizes MHP materials and devices. This study provides a fundamental insight into the structural and mechanical properties of perovskite grains, and points out a new direction to intrinsically enhance the perovskite stability, and then boost MHP electronic devices for commercial viability.

Introduction

Solar cells based on metal halide perovskites (MHPs) have shown high efficiencies of up to 25.2%,[1] which continue to compete with other photovoltaic technologies with promising future to further drive down the cost of clean solar energy.[2–8] Nevertheless, the stability of MHP solar cells remains to be one of the biggest barriers for the commercialization of this technology, and thus stabilizing the soft MHPs is crucial for continuing the development of MHP materials for photovoltaic applications.[9,10] In the past few years, the operational stability of MHP solar cells has been significantly improved with multi-facet strategies such as tuning the composition of the perovskites[11–15] and passivating defects at the film surface and grain boundaries for enhanced perovskite intrinsic stability,[16–18] improving the stability of charge transport layers which also impact the perovskite material and device stability,[19–25] and better encapsulation at both the grain level and device level.[26,27] However, the stability of perovskite solar cells is still far worse than that of commercial silicon solar cells, and thus much more improvement is required before the perovskite solar cells can become commercially viable.

[a] *Department of Applied Physical Sciences, University of North Carolina, Chapel Hill, NC 27599, USA. E-mail: jhuang@unc.edu*

[b] *Department of Mechanical and Materials Engineering and Nebraska Center for Materials and Nanoscience, University of Nebraska-Lincoln, Lincoln, Nebraska 68588, USA*

† Electronic supplementary information (ESI) available. See DOI: 10.1039/d1ee00116g

‡ These authors contributed equally to this work.

Enhancing the intrinsic stability of MHPs is clearly critical toward more stable devices, while the defect-less single crystalline form should represent its thermodynamically upper limit for the stability of a perovskite with known composition. It has been frequently observed by us that MHP single crystals can survive much longer than polycrystalline films under various stimuli. The difference in the grain size may explain the difference of the degradation behavior between polycrystalline films and single crystals. For example, scaling behavior has been observed in the degradation of perovskite films in moisture environments where degradation predominately occurs at grain boundaries.[28] One question that arises is whether there is some other hidden factor(s) besides the grain size, which obviously affects the degradation of MHPs.

Here we report the discovery of a layer of nanocrystals and amorphous phase of perovskites at the top surface of MHP polycrystalline thin films deposited by almost all known solution-process methods, and these nanocrystals and amorphous phase can initialize and accelerate the degradation of perovskite films. After removing the surface defective layer by mechanical polishing, the perovskite films show comparable mechanical properties with single crystal counterparts and significantly improved stability under illumination under ambient conditions compared to as-cast perovskite films. Polishing-off the surface defective layer not only effectively suppresses ion migration within MHP thin films and stabilizes perovskite materials, but also increases device efficiencies. Encapsulated solar cells based on polished MHP layers exhibited a small degradation by 1.5% relative to the initial efficiency after continuous illumination at 1 sun light intensity with ultra-violet (UV) radiation for 1000 h in air at 65 °C, and still retained 93% of its initial efficiency after illumination for three months.

Results and discussion

While we explored the mechanical polishing technology to optimize MHP thin films for high performance optoelectronic devices, we surprisingly found that mechanically polished $MAPbI_3$ ($MA = CH_3NH_3$) thin films were much more stable than unpolished as-cast $MAPbI_3$ thin films under continuous illumination at ambient air by a plasma lamp with strong ultraviolet and near infrared radiation at one-sun light intensity.[21] The ChemoMet soft pad with a porous structure (Fig. S1, ESI†) was used here. The video of a typical polishing process for MHP thin films can be found in the Supplementary video (ESI†). To avoid the influence of perovskite film morphology variation on the stability comparison, we polished only half side of each perovskite thin film while kept the other half side unpolished. It has been established that $MAPbI_3$ decomposes to PbI_2, and other species like CH_3I, NH_3, I_2 and H_2 *etc.*, under illumination in air, resulting in de-coloring of the films.[29–31] As shown in the photographs in Fig. 1A, the polished half side of the $MAPbI_3$ film degraded obviously slower than the non-polished half side of the same sample. To find out whether this phenomenon is dependent on the film deposition method, we measured the stability of $MAPbI_3$ thin films deposited by several different widely-used solution process methods, including the anti-solvent method by using varied dripping solvents (toluene and ethyl acetate),[32] air-quenched one-step spin-coating method,[33] vacuum-assisted one-step spin-coating method,[34] two-step inter-diffusion method,[35] and blade coating method at high temperature[36] and room temperature.[37] It was found that the non-polished half of all $MAPbI_3$ films degraded obviously faster than the polished half of the same thin film, regardless of the film deposition methods as shown in Fig. S2 (ESI†). We also tested the light soaking stability of $MAPbI_3$ films with different polishing-depths. As shown in Fig. S3 (ESI†), the films polished by 96 nm and 118 nm showed better stability than the one polished by 42 nm. This can be explained by the relatively large roughness of perovskite films. We further checked the stability of the MHP thin films under light with other compositions. $Cs_{0.4}FA_{0.6}Pb(I_{0.64}Br_{0.36})_3$ ($FA = HC(NH_2)_2$) (denoted as CsFA-perovskite hereinafter) and $FA_{0.81}MA_{0.14}Cs_{0.05}PbI_{2.55}Br_{0.45}$ (CFM-perovskite) thin films showed much better stability than $MAPbI_3$. Both polished CsFA-perovskite and CFM-perovskite thin films showed better stability than unpolished areas under illumination in ambient air, as shown by the light soaking results in Fig. 1A. These results conclude that the spontaneously formed layers accelerate the degradation of perovskites, while removing the surface layer by a simple mechanical polishing can make these MHP thin films much more stable under illumination. In addition, the thermal stability and moisture stability of the MHP films with and without polishing have also been investigated. After thermal annealing at 60 °C for 18 h and then 110 °C for 25 h in the dark and in air, the polished half side of the MHP thin film did not show better thermal stability than the unpolished half side (Fig. S4, ESI†). Relative to the unpolished MHP thin film, the polished sample did not show obviously better moisture stability in the dark and under nitrogen conditions as shown in Fig. S5 (ESI†).

To evaluate the impact of the polishing surface on the stability of solar cells based on MHP thin films, the operational stabilities of MHP solar cells with and without polishing were compared. The devices have a p–i–n planar structure of indium tin oxide (ITO)/poly[bis(4-phenyl)(2,4,6-trimethylphenyl)amine] (PTAA)/MHP/C_{60}/bathocuproine (BCP)/copper (Cu) without and with [6,6]-phenyl-C_{61}-butyric acid methyl ester (PCBM) or oxysalt passivation layers, and were encapsulated before the stability test. PCBM and oxysalt have been reported to passivate the defects in perovskite thin films, and oxysalt passivation improves the device stability due to the formation of strong chemical bonds of Pb^{2+} and SO_4^{2-}. The device stability was measured under operating conditions under a plasma lamp with a light intensity of 100 mW cm^{-2}, and a similar spectrum to AM 1.5 G light and strong UV components.[21] The devices were connected to a load so that they operate at the maximum power point (MPP) at the beginning of the test. The load was then fixed for the duration of the measurement, which might slightly underestimate the stability of the solar cells since the MPP moves during the test. The stability testing was conducted in air, and the surface of the devices showed a stabilized temperature of ~65 °C under

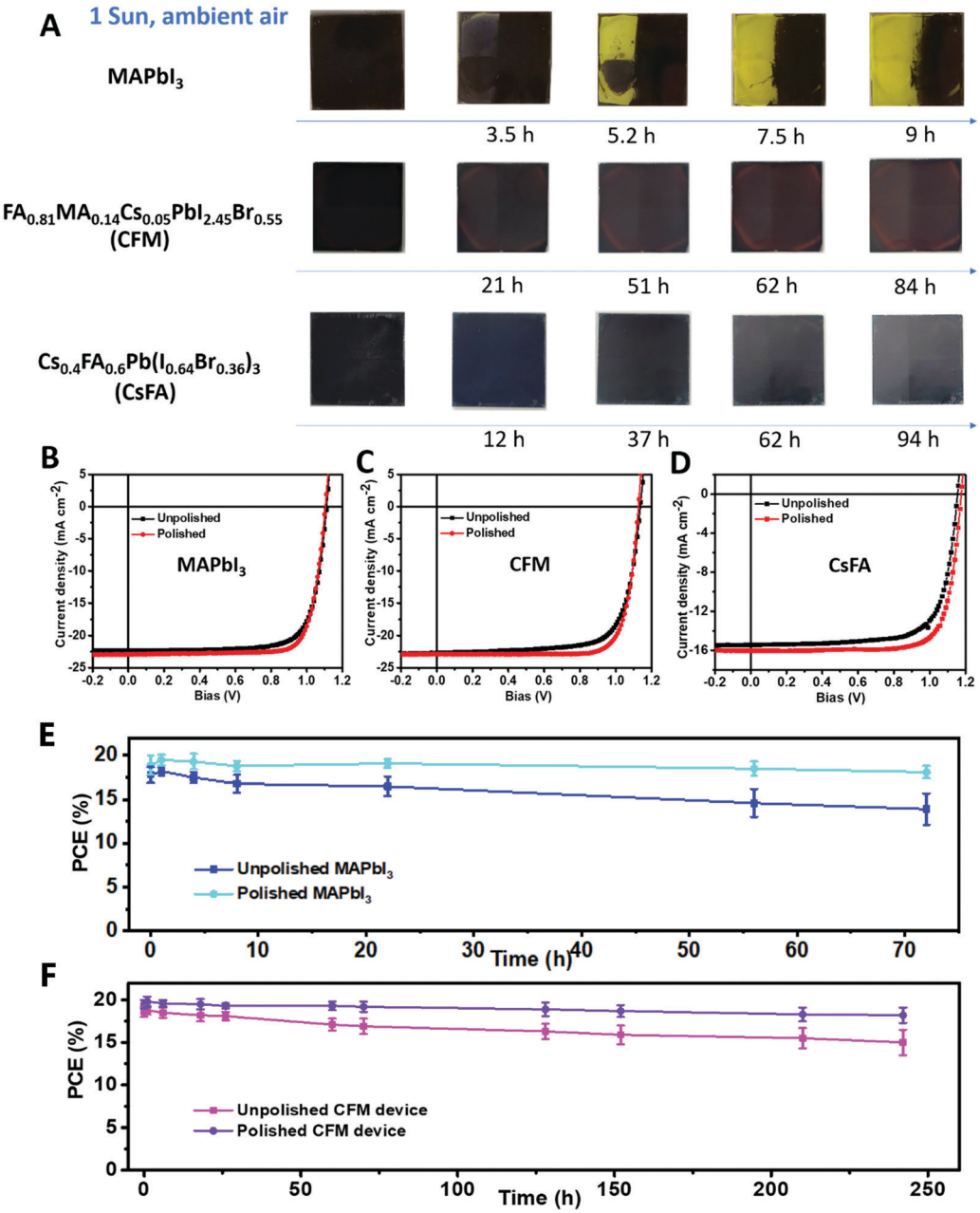

Fig. 1 The effect of polishing on the stability of MHP thin films and solar cells. (A) Photographs of the $MAPbI_3$ deposited by the anti-solvent method with ethyl acetate dripping, CFM-perovskite and CsFA-perovskite thin films after illumination for different durations under light intensity of 100 mW cm^{-2} in ambient air. The right half sides of all samples were polished before the light stability test. The *J–V* curves of solar cells based on (B) $MAPbI_3$, (C) CFM, and (D) CsFA thin films without and with polishing treatment. The light stability of the encapsulated devices of solar cells based on (E) $MAPbI_3$, and (F) CFM thin films without and with polishing treatment, with the PCBM passivation layer, under continuous illumination at one-sun intensity. Five devices were tested.

continuous illumination, while it was likely that the perovskite layer had a higher temperature. As shown in Fig. 1B–D, Fig. S6 and Table S1 (ESI†), the solar cells based on polished perovskites with varied compositions showed higher PCEs than the control devices with as-cast MHP thin films, which indicates that the spontaneously formed surface layers also reduce the device efficiency. Polished $MAPbI_3$ devices showed no negligible difference from *J–V* scanning at different directions and speeds, and with and without the photomask, and the calculated J_{SC} from EQE matched well with that from *J–V* scanning (Fig. S7, ESI†). The PCBM-passivated solar cells with polished $MAPbI_3$ thin films exhibited better light stability compared to the control devices (Fig. 1E). After continuous illumination for 72 h, the PCEs of solar cells based on polished $MAPbI_3$ decreased by 3.8% on average. In contrast, the devices with pristine $MAPbI_3$ showed a much large PCE loss of 22% under the same test conditions. The same trend of increased stability after polishing was also observed in solar cells with CFM-perovskite thin films and PCBM passivation. After continuous illumination

for 242 hours (Fig. 1F), the PCEs of the devices with unpolished CFM-perovskite decreased by 20% on average, while the polished ones showed a decrease of PCE by only 6.7% on average. The stability of solar cells with polished CFM films was further improved by using a wide bandgap oxysalt layer to replace PCBM which further stabilizes the perovskite surfaces.[21] It can be seen that polishing further improved the device stability of oxysalt-passivated devices to a new high level, in addition to slightly enhancing the device efficiency (Fig. S8A, ESI†). Fig. 2 shows the evolution of open circuit voltage (V_{OC}), short-circuit current (J_{SC}), fill factor (FF) and PCE of the oxysalt-passivated CFM perovskite solar cells with and without polishing. The oxysalt-passivated solar cells with polishing treatment showed 3% degradation on average relative to the original PCE after continuous illumination for ~1000 h, while the unpolished devices lost 8.7% of their efficiency on average. The polished device combined with the oxysalt layer, which showed the best stability under continuous illumination, had an initial PCE of 20.4% (Fig. S8B, ESI†) estimated from the stabilized output. This device retained about 98.5% of its initial PCE after continuous illumination for 1000 h. After testing for 2180 h which is more than 3 months, the device still retained 93% of its initial PCE (Fig. 2). This represent the best reported operational stability for perovskite solar cells with PCEs more than 20%.[14,15,17,19,21–23,25–27,38,39] We also applied this method to treat the surface of polycrystalline $CsPbBr_3$ perovskite light emitting diodes (LEDs). The details of the material, structure and fabrication of light emitting diodes can be found in the ESI.† Polishing the surface of a perovskite thin film is also shown as an effective method to significantly enhance the operational stability of perovskite LEDs by extending the T_{50} lifetime by three times (*i.e.* the time it takes for the luminance to decrease by half of the original value) (Fig. S9, ESI†).

To understand why the stability of perovskite films and devices was significantly enhanced by polishing, we investigated the effect of polishing on the surface morphology, optoelectronic and mechanical properties of MHPs. XPS results showed that polishing did not induce other elements (such as Si) from the ChemoMet polishing pad (Fig. S10B and C, ESI†) or obviously

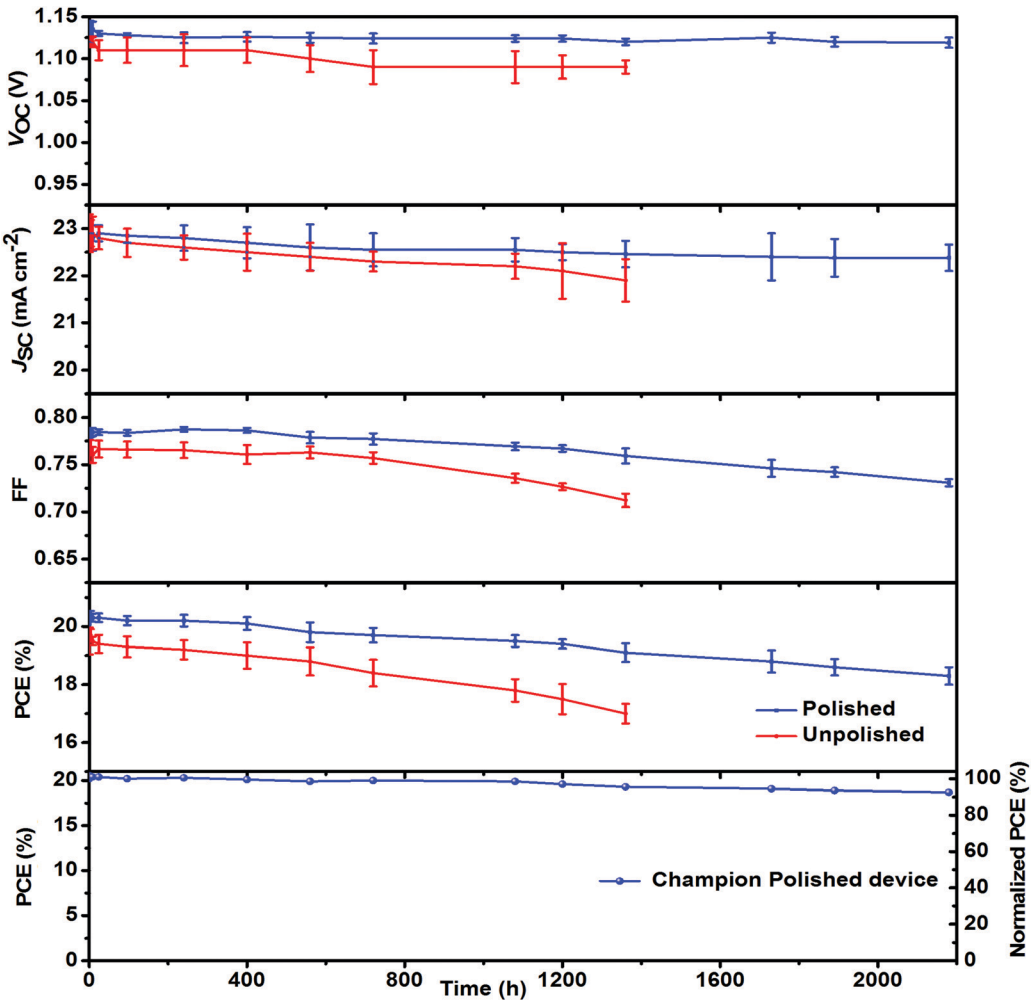

Fig. 2 Enhanced device stability by polishing. The device parameter evolution of encapsulated solar cells based on unpolished and polished $FA_{0.81}MA_{0.14}Cs_{0.05}PbI_{2.45}Br_{0.55}$ (CFM) with octylammonium sulfate passivation under continuous illumination at one sun intensity, which is tested in air, with UV and at around 65 °C. Five devices were tested. Except the bottom figure which showed the champion stability of the polished device, the other figures showed the mean values with standard deviations.

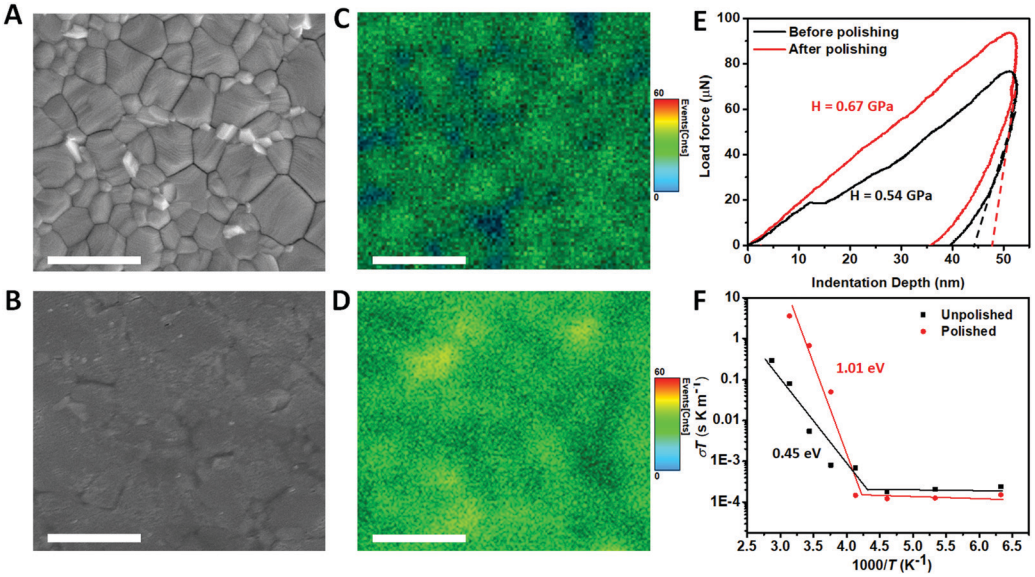

Fig. 3 Morphology, optical, mechanical and ion migration properties of perovskite films before and after polishing-off the defective surface. (A and B) Top-view SEM images of a $MAPbI_3$ thin film (A) before and (B) after polishing. (C and D) Photoluminescence intensity mapping images for a $MAPbI_3$ thin film (C) before and (D) after polishing treatment. All the scale bar for A–D is 1 μm. (E) Nanoindentation measurement result of $MAPbI_3$ thin film surface before and after polishing with a maximum indentation depth of 50 nm. (F) Ion migration activation energy of $MAPbI_3$ thin films without and with polishing treatment.

shift the N, Pb, and I peaks of the perovskite thin film (Fig. S10D–F, ESI†), which can exclude the potential effect on the stability of surface modification from materials of the polishing pad. As shown by the top-view scanning electron microscopy (SEM) images in Fig. 3A and B, the polished film is more uniform and flatter than the as-cast thin film. The SEM studies showed that most area at the spontaneously formed surface of MHP thin films should be removed by polishing off about 142 nm, as shown by the cross-sectional SEM images in Fig. S11 (ESI†). The $MAPbI_3$ film before polishing exhibited obvious "V-shaped" grain boundaries, while after polishing it retained dense grain packing after exposure to the electron beam in SEM. We mapped the photoluminescence (PL) intensity of the $MAPbI_3$ thin film before and after polishing using a confocal optimal mapping system. As shown in Fig. 3C and D, the PL intensity of the $MAPbI_3$ film has increased after polishing within a randomly chosen detection region with an area of 10 μm × 10 μm, and PL mapping showed a more uniform surface on the polished perovskite, which benefited the device FF improvement.

The mechanical property characterization of perovskite thin films before and after polishing the surface was compared by nanoindentation measurements. Here we measured 24 locations which were randomly chosen among different samples. As shown in Fig. 3E, the hardness (H) at the top surface of $MAPbI_3$ thin films increased from 0.54 ± 0.14 GPa to 0.67 ± 0.04 GPa after polishing with an indentation depth of 50 nm. The hardness of the polished $MAPbI_3$ thin films is very close to that of the $MAPbI_3$ single crystal (H = 0.69 ± 0.12 GPa from measurement at 9 locations with an indentation depth of 600 nm on bulk crystals of 1–5 mm thick), as shown in Fig. S12 (ESI†). The single-crystal-like mechanical properties of polished $MAPbI_3$ thin films indicated that polishing could recover the mechanical properties of the perovskite thin films to the quality of perovskite single crystals. The same trend of increased hardness by polishing treatment was observed in MHP films with other compositions, and the statistical results are shown in Table S2 and Fig. S13 (ESI†).

A harder surface of polished perovskite thin films is expected to reduce the ion migration along the surface layer of the perovskite. The more robust and less porous surface after polishing should result in suppressed ion migration at the perovskite thin film which is arguably the most difficult aspect to address. To investigate whether polishing-off the MHP surface suppresses the ion migration of perovskite films, we measured the activation energy (E_a) for ion migration of MHPs before and after mechanical polishing-off defective MHP surfaces. We used a lateral device structure to highlight the ion migration at the MHP film surface. The activation energy of ion migration was extracted from the dependence of the conductivity of the $MAPbI_3$ films on temperature. The temperature dependent conductivity shows a clear two-stage variation which can be assigned to electronic and ionic conduction as established from previous studies. In Fig. 3F, the as-prepared $MAPbI_3$ films showed an E_a of 0.38 ± 0.1 eV for ion migration, while the polished $MAPbI_3$ films showed a much larger E_a of 0.88 ± 0.15 eV under dark conditions. These higher E_a values indicated that polishing efficiently suppressed the ion migration of MHPs. The E_a of the polished film is comparable to that of $MAPbI_3$ single crystals, which is consistent with single-crystal-like mechanical properties of polished MHP thin films.[40] These results confirm that polishing-off the soft surface of perovskite thin films makes the surface of polycrystalline MHP thin films hard as single crystals and greatly suppressed the ion migration of MHPs,

which contributed to the enhanced stability of MHP thin films and extended durability of perovskite photovoltaic devices.

The next question left to be addressed is why the spontaneously formed defective surface of perovskite thin films is softer than the underneath crystals and accelerates the degradation of perovskites. Previous studies by high resolution transmission electron microscopy (HRTEM) revealed that some grain boundaries of polycrystalline films had an amorphous region which allowed the fast permeation of moisture and other hazards.[28] We hypothesize that the surface of some perovskite grains might have similar morphology to grain boundaries, and thus examined the morphology of MHP polycrystalline thin films by cross-sectional HRTEM. To prepare the sample, high efficiency devices made of polycrystalline films, such as $MAPbI_3$ based devices with over 20% efficiencies, were chosen. These devices have a structure of ITO/PTAA/MHPs/C_{60}/BCP/Cu. The samples for HRTEM were prepared using the focused ion beam (FIB) technique with small gallium ion beam current (28–48 pA) and low voltage (5 kV), which has been shown in previous studies to minimize the damage induced by ion beams and thus provide clear HRTEM images.[41,42] TEM images as shown in Fig. 4A, C and D were acquired at 5 different depths from a $MAPbI_3$ perovskite grain surface (*i.e.* C_{60}/MHP interface) to the interior with locations labeled in Fig. 4A. The crystallographic orientation of the lattice at each location was determined by fast Fourier transformation (FFT) of the lattice, which are shown by the insets of the images in Fig. 4C. Fig. 4C shows that single crystalline $MAPbI_3$ with an interplanar spacing of 3.1 Å is clearly present at locations inside the perovskite grain, corresponding to the (220) plane of $MAPbI_3$. There is no change of crystallographic orientation or any extended defect such as dislocations or twin boundaries from grain interior up to the region of tens of nanometers below the top surface inside the single-grain. In striking contrast, the top surface of the $MAPbI_3$ layer with a thickness of 30–50 nm (region 1 shown in Fig. 4A and C) is mostly composed of many nanocrystals, which are circled by yellow dashed lines in Fig. 4C and D. Some areas without clear crystalline structures from FFT images are referred to as amorphous phase regions. To verify whether this phenomenal is general, we scanned multiple randomly selected locations near the $MAPbI_3/C_{60}$ interface at region 1 (marked in Fig. 4A). The HRTEM images are shown in Fig. 4D. Again, both nanocrystals and amorphous regions were observed at the top surface of $MAPbI_3$ at every location measured. Some locations at interface region 1 exhibited other interplanar spacings of 2.2 Å that corresponds to the crystal plane (224) in Fig. 4C and 3.6 Å that corresponds to the crystal plane (202) as shown in Fig. 4D. The morphology study concludes the presence of a large density of defective regions close to the $MAPbI_3$ film top surface area, which is illustrated in Fig. 4B. Then we tested whether a mechanical polishing process using the ChemoMet soft pad could remove the surface defective layer. Atomic force microscopy (AFM) images (Fig. S14, ESI†) showed the smoother surface of the perovskite thin film polished by ChemoMet Pad with a root-mean-square (RMS) roughness of 9 nm, smaller than that (20 nm) of unpolished perovskite thin films. HRTEM images as shown in Fig. 5A, C and D were acquired at 5 different depths from the surface of a polished $MAPbI_3$ perovskite film. Fig. 5C shows that both at the surface and inside the perovskite grains single crystalline structures are present with an interplanar spacing of 3.1 Å corresponding to the (220) plane. In contrast to the as-cast perovskite films, the top surface of the polished $MAPbI_3$ layer did not show any nanocrystals or amorphous region, as shown in Fig. 5C and D. These results directly confirmed that the applied polishing process can efficiently remove the surface defective nanostructured layer. In addition, X-ray photoelectron spectroscopy (XPS) and grazing incidence X-ray diffraction (GIXRD) measurements were also conducted to investigate the chemical and structural properties of the top surface layer of $MAPbI_3$ thin films without and with polishing. From XPS results shown in Fig. S10 (ESI†), the unpolished $MAPbI_3$ surface showed a molar ratio of N : Pb : I of 0.6 : 1 : 2.2. In contrast, the polished perovskite surface showed a N : Pb : I ratio of 0.8 : 1 : 2.7, which is much closer to the stoichiometry ratio (1 : 1 : 3) of $MAPbI_3$. These results indicate that more defects, such as MA vacancies, I vacancies, *etc.*, existed on the surface of the as-cast $MAPbI_3$ films. In GIXRD measurements, the X-ray beam came in at a very small angle to reveal the structure of the perovskite surface within several nanometers thickness. Fig. S15A (ESI†) shows the X-ray penetration depth *versus* X-ray incident angle, giving an X-ray penetration depth of about 5 nm into $MAPbI_3$ with an incident angle of 0.3°. The GIXRD patterns (Fig. S15B, ESI†) showed that the PbI_2 existed on the surfaces of unpolished perovskite films, but disappeared from the surfaces of polished perovskite films. This result is consistent with the XPS analysis of elements ratio, because polishing off the nanostructured defective layer which is rich with PbI_2 made the N : Pb : I ratio on surface much closer to the stoichiometry ratio of $MAPbI_3$. GIXRD analysis, as well as XPS, supported the presence of defective layers on unpolished perovskite films concluded from the HRTEM study, and the polishing process effectively removed these surface defective layers.

To further investigate whether the defective surface layers composed of nanocrystals and amorphous phase only exist on $MAPbI_3$ films, we obtained the cross-sectional HRTEM images of a MA-free perovskite with composition of CsFA-perovskite polycrystalline thin films without and with polishing, which are shown in Fig. S16 and S17 (ESI†). For the HRTEM study, six different locations, two at the C_{60}/CsFA-perovskite interface and four inside the perovskite film, in each CsFA-perovskite device were selected, with all locations marked in Fig. S16 and S17 (ESI†). At each of the 6 locations, there were 6 zoomed-in images with an area of 100 nm^2 at different positions, which results in 36 HRTEM images for each sample. The X-ray diffraction pattern of the CsFA-perovskite films in Fig. S18 (ESI†) shows that the (110) planes have the strongest peak, therefore we kept tracking the (110) crystal planes in HRTEM images, which correspond to a crystal plane spacing of 4.3 Å. In the region close to the C_{60}/CsFA-perovskite interface as shown in Fig. S16B (ESI†), many randomly oriented nanocrystals and amorphous regions were observed. We observed blurred amorphous regions in many zoomed-in locations (1), (3), (5), at region I and (6)

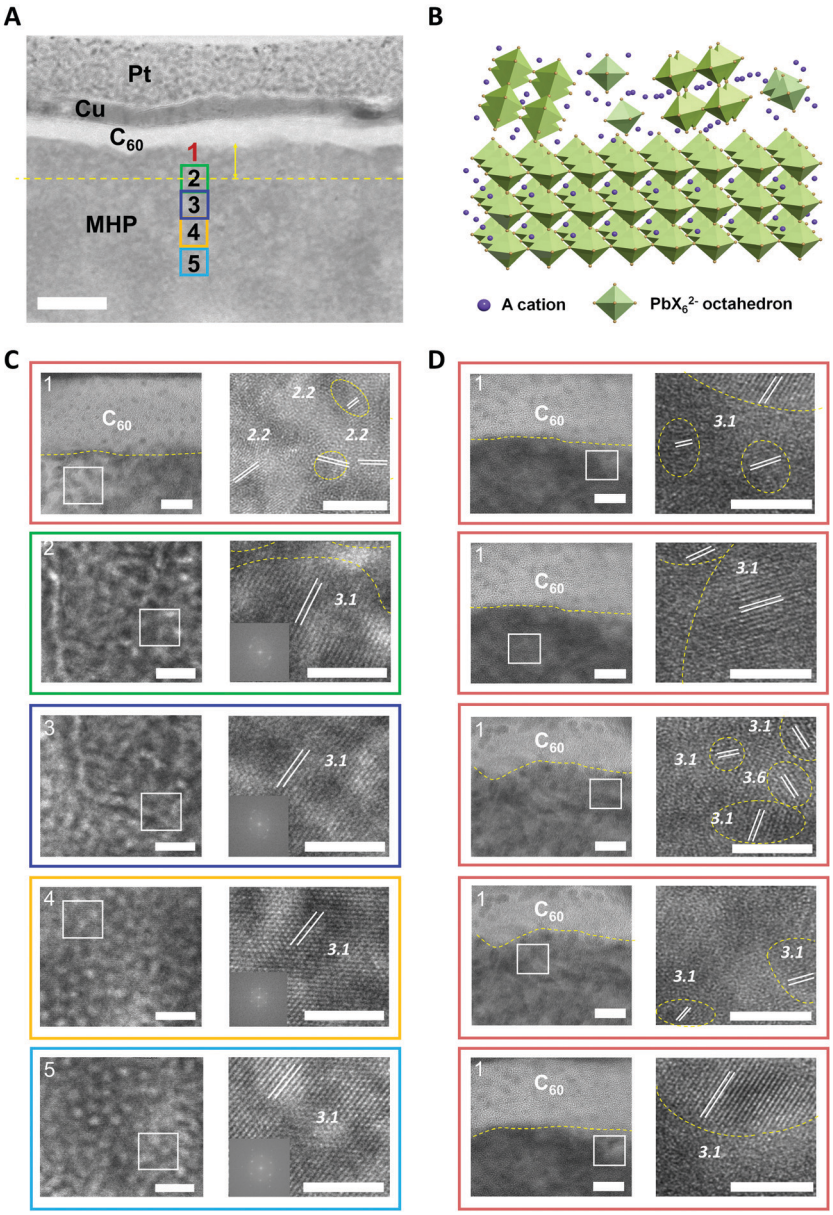

Fig. 4 Morphology at the top surface of $MAPbI_3$ thin films. (A) Cross-sectional TEM image of a device with a structure of ITO/PTAA/$MAPbI_3$/C_{60}/BCP/Cu. The interface area of region 1 is marked in red color. Locations of 2–5 are marked by the squares for zoom-in HRTEM measurement. The scale bar is 100 nm. (B) Schematic illustration of the nanocrystals and amorphous-phase at the top surface of MHP polycrystalline films. (C) HRTEM images of $MAPbI_3$ at different positions of 1–5 labelled in (A), and (D) the HRTEM images of another five positions randomly selected at the interface of $MAPbI_3$ and C_{60}. All the scale bars in the left column are 10 nm, and all the scale bars in the right column are 5 nm. The areas marked in white squares in left columns are zoomed in the right columns. The boundaries of nanocrystals, as well as the boundaries between perovskite and C_{60} in (C and D), are marked in yellow dashed lines.

at region VI, and other crystalline regions with different crystallographic planes of (200) and (210) at regions I and VI, which exhibit crystal plane spacing of 3.1 Å and 2.7 Å, respectively. From the interface regions to the grain interiors shown in Fig. S16B–D (ESI†), randomly oriented nanocrystals and amorphous regions gradually reduced, and then the grain interiors (Fig. S16D, ESI†) show good crystallinity with no notable change of crystallographic orientation identified in a single grain of the CsFA-perovskite. After polishing off the top layer by about 40 nm, the perovskite grain interiors (Fig. S17C and D, ESI†) retained good crystallinity with continuous (110) crystal planes, and most of the randomly oriented nanocrystals and amorphous-phase regions on the surface are removed, as shown in Fig. S17B (ESI†), and no additional damage was found to have caused by polishing. This result meant that the nanocrystals and amorphous phase generally formed on the top surface of perovskite films independent of the MHP composition. The presence of defective nanocrystals and amorphous phase at the perovskite surface induced more open and defective structures similar to grain boundaries, leading to decreased surface hardness and moisture and oxygen permeation into the perovskite films, and faster ion migration in the perovskite film. Then the degradation of devices based on perovskite thin

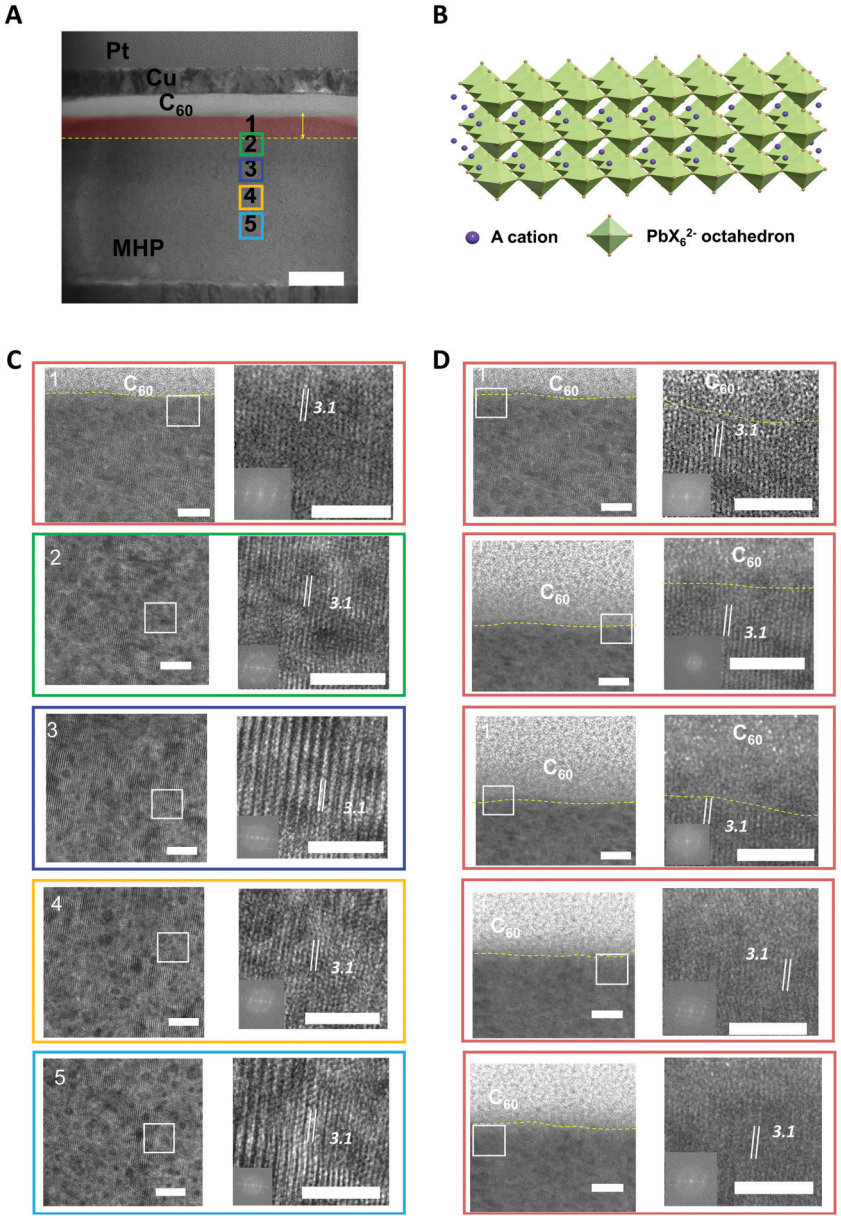

Fig. 5 Morphology at the top surface of polished $MAPbI_3$ thin films. (A) Cross-sectional TEM image of a device with a structure of ITO/PTAA/polished $MAPbI_3$/C_{60}/BCP/Cu. The interface area of region 1 is marked in red color. Locations of 2–5 are marked by the squares for zoom-in HRTEM measurements. The scale bar is 100 nm. (B) Schematic illustration of the top surface of polished MHP polycrystalline films. (C) HRTEM images of polished $MAPbI_3$ at different positions of 1–5 labelled in (A), and (D) the HRTEM images of another five positions randomly selected at the interface of polished $MAPbI_3$ and C_{60}. All the scale bars in the left column are 10 nm, and all the scale bars in the right column are 5 nm. The areas marked in white squares in left columns are zoomed in in the right columns. The boundaries between perovskite and C_{60} in (C and D) are marked in yellow dashed lines.

films starts from defective sites on the soft surface, because the presence of charge traps can increase the ion migration and degradation of perovskites,[40,43–48] and the stability of perovskite thin films and devices is significantly improved after polishing the perovskite surface. The degradation process produced by-products such as PbI_2 which has been reported to act as a catalyst to further enhance the degradation of perovskite films.[49] In addition, the degradation of the defective layer should also cause lattice distortion at the interface degraded region and pristine region due to the mismatched lattice constant or permeation of moisture and oxygen, which deserves further study by *in situ* characterization. So once the surface degradation occurs, the degradation products would further accelerate the degradation of the crystalline region under illumination, which would result in the degradation of the whole films.

Conclusions

In summary, we demonstrated that removing the defective layer by mechanical polishing could make MHP polycrystalline materials behave close to single crystals with enhanced hardness and reduced ion migration, which effectively stabilized

perovskite thin films and solar cells. This method is broadly applicable to other perovskite materials and devices. Then we found the presence of a large density of disconnected small crystals with sizes of nanometers and some amorphous phases at the surface of polycrystalline MHP films, which limit the improvement of stability of halide perovskite thin films. Although polishing itself is not a low-cost method in industrial large area perovskite solar panel manufacturing, this study provides fundamental insights into the structural and mechanical properties of perovskite grains that cause the degradation of MHP polycrystalline films, and points out a new direction to intrinsically stabilize perovskite materials and devices.

Author contributions

Y. Lin and Y. Liu contributed equally to this work. J. H. and Y. Lin conceived the idea and designed the experiments. Y. Lin fabricated perovskite thin films and devices, polished perovskite samples, and measured their stabilities. Y. Liu developed the polishing method for perovskite thin films, polished perovskite samples and measured the mechanical properties. S. C. and S. W. conducted and analyzed TEM. S. W. conducted and analyzed XPS measurement. J. Z conducted and analyzed GIXRD. S. Y. synthesized octylammonium sulfate. Z. Y. contributed to the fabrication of perovskite films and devices. C. H. B and Z. N. measured and analyzed PL intensity mapping. X. D. and S. C. conducted SEM measurements. Y. D. contributed to blade perovskite thin films. Q. W. fabricated light emitting diodes and determined the stability. J. H. and Y. Lin and Y. Liu wrote the paper. All authors reviewed this paper.

Conflicts of interest

The authors declare no competing interests.

Acknowledgements

This work is supported by Office of Naval Research under the awards N00014-17-1-2727 and N00014-18-1-2239. This work was performed in part at the Analytical Instrumentation Facility (AIF) at North Carolina State University and Chapel Hill Analytical and Nanofabrication Laboratory at University of North Carolina at Chapel Hill, which is supported by the State of North Carolina and the National Science Foundation (award number ECCS-1542015).

References

1 National Renewable Energy Laboratory, Best research-cell efficiencies chart https://www.nrel.gov/pv/cell-efficiency.html, 2020.
2 A. Kojima, K. Teshima, Y. Shirai and T. Miyasaka, Organometal halide perovskites as visible-light sensitizers for photovoltaic cells, *J. Am. Chem. Soc.*, 2009, **131**, 6050–6051.
3 H.-S. Kim, *et al.*, Lead iodide perovskite sensitized all-solid-state submicron thin film mesoscopic solar cell with efficiency exceeding 9%, *Sci. Rep.*, 2012, **2**, 591.
4 M. M. Lee, J. Teuscher, T. Miyasaka, T. N. Murakami and H. J. Snaith, Efficient hybrid solar cells based on meso-superstructured organometal halide perovskites, *Science*, 2012, **338**, 643–647.
5 H. Zhou, *et al.*, Interface engineering of highly efficient perovskite solar cells, *Science*, 2014, **345**, 542–546.
6 J. Burschka, *et al.*, Sequential deposition as a route to high-performance perovskite-sensitized solar cells, *Nature*, 2013, **499**, 316.
7 E. H. Jung, *et al.*, Efficient, stable and scalable perovskite solar cells using poly (3-hexylthiophene), *Nature*, 2019, **567**, 511–515.
8 Q. Jiang, *et al.*, Surface passivation of perovskite film for efficient solar cells, *Nat. Photonics*, 2019, **13**, 460–466.
9 Y. Yang and J. You, Make perovskite solar cells stable, *Nature*, 2017, **544**, 155–156.
10 L. Meng, J. You and Y. Yang, Addressing the stability issue of perovskite solar cells for commercial applications, *Nat. Commun.*, 2018, **9**, 5265.
11 Z. P. Wang, *et al.*, Efficient ambient-air-stable solar cells with 2D–3D heterostructured butylammonium-caesium-formamidinium lead halide perovskites, *Nat. Energy*, 2017, **2**, 17135.
12 G. Grancini, *et al.*, One-Year stable perovskite solar cells by 2D/3D interface engineering, *Nat. Commun.*, 2017, **8**, 15684.
13 H. Tsai, *et al.*, High-efficiency two-dimensional Ruddlesden–Popper perovskite solar cells, *Nature*, 2016, **536**, 312–316.
14 L. Wang, *et al.*, A Eu^{3+}-Eu^{2+} ion redox shuttle imparts operational durability to Pb-I perovskite solar cells, *Science*, 2019, **363**, 265–270.
15 S.-H. Turren-Cruz, A. Hagfeldt and M. Saliba, Methylammonium-free, high-performance, and stable perovskite solar cells on a planar architecture, *Science*, 2018, **362**, 449–453.
16 X. Zheng, *et al.*, Defect passivation in hybrid perovskite solar cells using quaternary ammonium halide anions and cations, *Nat. Energy*, 2017, **2**, 17102.
17 S. Bai, *et al.*, Planar perovskite solar cells with long-term stability using ionic liquid additives, *Nature*, 2019, **571**, 245–250.
18 M. Abdi-Jalebi, *et al.*, Maximizing and stabilizing luminescence from halide perovskites with potassium passivation, *Nature*, 2018, **555**, 497.
19 H. Tan, *et al.*, Efficient and stable solution-processed planar perovskite solar cells via contact passivation, *Science*, 2017, **355**, 722–726.
20 D. Luo, *et al.*, Enhanced photovoltage for inverted planar heterojunction perovskite solar cells, *Science*, 2018, **360**, 1442–1446.
21 S. Yang, *et al.*, Stabilizing halide perovskite surfaces for solar cell operation with wide-bandgap lead oxysalts, *Science*, 2019, **365**, 473–478.
22 J. A. Christians, *et al.*, Tailored interfaces of unencapsulated perovskite solar cells for >1,000 hour operational stability, *Nat. Energy*, 2018, **3**, 68–74.
23 S. S. Shin, *et al.*, Colloidally prepared La-doped $BaSnO_3$ electrodes for efficient, photostable perovskite solar cells, *Science*, 2017, **356**, 167–171.

24 W. Chen, *et al.*, Efficient and stable large-area perovskite solar cells with inorganic charge extraction layers, *Science*, 2015, **350**, 944–948.

25 N. Arora, *et al.*, Perovskite solar cells with CuSCN hole extraction layers yield stabilized efficiencies greater than 20%, *Science*, 2017, **358**, 768–771.

26 Y. Bai, *et al.*, Oligomeric silica-wrapped perovskites enable synchronous defect passivation and grain stabilization for efficient and stable perovskite photovoltaics, *ACS Energy Lett.*, 2019, **4**, 1231–1240.

27 F. Bella, *et al.*, Improving efficiency and stability of perovskite solar cells with photocurable fluoropolymers, *Science*, 2016, **354**, 203–206.

28 Q. Wang, *et al.*, Scaling behavior of moisture-induced grain degradation in polycrystalline hybrid perovskite thin films, *Energy Environ. Sci.*, 2017, **10**, 516–522.

29 S. Wang, *et al.*, Accelerated degradation of methylammonium lead iodide perovskites induced by exposure to iodine vapour, *Nat. Energy*, 2017, **2**, 16195.

30 E. J. Juarez-Perez, Z. Hawash, S. R. Raga, L. K. Ono and Y. Qi, Thermal degradation of $CH_3NH_3PbI_3$ perovskite into NH_3 and CH_3I gases observed by coupled thermogravimetry–mass spectrometry analysis, *Energy Environ. Sci.*, 2016, **9**, 3406–3410.

31 E. J. Juarez-Perez, L. K. Ono, I. Uriarte, E. J. Cocinero and Y. Qi, Degradation mechanism and relative stability of methylammonium halide based perovskites analyzed on the basis of acid–base theory, *ACS Appl. Mater. Interfaces*, 2019, **11**, 12586–12593.

32 N. J. Jeon, *et al.*, Solvent engineering for high-performance inorganic–organic hybrid perovskite solar cells, *Nat. Mater.*, 2014, **13**, 897–903.

33 F. Huang, *et al.*, Gas-assisted preparation of lead iodide perovskite films consisting of a monolayer of single crystalline grains for high efficiency planar solar cells, *Nano Energy*, 2014, **10**, 10–18.

34 X. Li, *et al.*, A vacuum flash–assisted solution process for high-efficiency large-area perovskite solar cells, *Science*, 2016, **353**, 58–62.

35 Z. Xiao, *et al.*, Efficient, high yield perovskite photovoltaic devices grown by interdiffusion of solution-processed precursor stacking layers, *Energy Environ. Sci.*, 2014, **7**, 2619–2623.

36 Y. Deng, *et al.*, Scalable fabrication of efficient organolead trihalide perovskite solar cells with doctor-bladed active layers, *Energy Environ. Sci.*, 2015, **8**, 1544–1550.

37 Y. Deng, *et al.*, Tailoring solvent coordination for high-speed, room-temperature blading of perovskite photovoltaic films, *Sci. Adv.*, 2019, **5**, eaax7537.

38 Y. Hou, *et al.*, A generic interface to reduce the efficiency-stability-cost gap of perovskite solar cells, *Science*, 2017, **358**, 1192–1197.

39 D. Bi, *et al.*, Multifunctional molecular modulators for perovskite solar cells with over 20% efficiency and high operational stability, *Nat. Commun.*, 2018, **9**, 4482.

40 S. P. Dunfield, *et al.*, From defects to degradation: A mechanistic understanding of degradation in perovskite solar cell devices and modules, *Adv. Energy Mater.*, 2020, **10**, 1904054.

41 M. Rothmann, *et al.*, Structural and chemical changes to $CH_3NH_3PbI_3$ induced by electron and gallium ion beams, *Adv. Mater.*, 2018, **30**, 1800629.

42 R. Garcia, F. A. Stevie and L. Giannuzzi, FIB sample preparation for in depth EDS analysis, *Microsc. Microanal.*, 2019, **25**, 914–915.

43 F. Wang, S. Bai, W. Tress, A. Hagfeldt and F. Gao, Defects engineering for high-performance perovskite solar cells, *npj Flexible Electron.*, 2018, **2**, 22.

44 N. Aristidou, *et al.*, Fast oxygen diffusion and iodide defects mediate oxygen-induced degradation of perovskite solar cells, *Nat. Commun.*, 2017, **8**, 15218.

45 N. Ahn, *et al.*, Trapped charge-driven degradation of perovskite solar cells, *Nat. Commun.*, 2016, **7**, 13422.

46 J. Xing, *et al.*, Ultrafast ion migration in hybrid perovskite polycrystalline thin films under light and suppression in single crystals, *Phys. Chem. Chem. Phys.*, 2016, **18**, 30484–30490.

47 Y. Shao, *et al.*, Grain boundary dominated ion migration in polycrystalline organic–inorganic halide perovskite films, *Energy Environ. Sci.*, 2016, **9**, 1752–1759.

48 Y. Yuan and J. Huang, Ion migration in organometal trihalide perovskite and its impact on photovoltaic efficiency and stability, *Acc. Chem. Res.*, 2016, **49**, 286–293.

49 B. Roose, K. Dey, Y.-H. Chiang, R. H. Friend and S. D. Stranks, Critical Assessment of the Use of Excess Lead Iodide in Lead Halide Perovskite Solar Cells, *J. Phys. Chem. Lett.*, 2020, **11**, 6505–6512.

